# CONTRIBUTION TO THE PV-TO-INVERTER SIZING RATIO DETERMINATION USING A CUSTOM FLEXIBLE EXPERIMENTAL SETUP

Xavier Camps, Guillermo Velasco[b], Jordi de la Hoz[a,*], Helena Martín[a]

[a]Department of Electrical Engineering, [b]Department of Electronic Engineering

Universitat Politècnica de Catalunya (UPC)

Escola Universitària d'Enginyeria Tècnica Industrial de Barcelona (EUETIB)

Carrer del Comte d'Urgell, 187, 08036, Barcelona, Spain

*Corresponding author. Tel.: +34 934 137 319; fax: +34 934 137 401

*E-mail address*: jordi.de.la.hoz@upc.edu (J. de la Hoz)

## Abstract

This work presents a novel approach to the experimental validation of the optimal PV-to- inverter sizing ratio value for the energy yield maximization of a GCPVS by means the implementation of a custom workbench using a solar array simulator which has allowed to replicate a wide variety of technical configurations and environmental data. The compliance between the experimental setup and the mathematical model developed to simulate the optimal PV-to- inverter sizing ratio value was demonstrated by the specific tests carried out on its two main subsystems (the PV generator and the inverter), thus the subsequent simulations were made on a firm basis. Likewise, the evaluation of the overall system also showed a good agreement between the experimental and the simulated *energy yield* and optimal PV-to-inverter sizing ratio results, rendering relative errors below 3% for both magnitudes.

## Keywords

PV-to-Inverter Sizing Ratio, Grid Connected PV Systems, Inverter, final Energy Yield Factor, Renewable Energy

## 1. Introduction

Photovoltaic (PV) energy is a secure, clean, renewable and environmentally friendly energy source. PV energy generation plays an important role worldwide and represents a growing renewable energy alternative. Nevertheless, although the cost of grid connected PV systems (GCPVS) has been decreasing over the time, their high capital cost when compared with conventional energy sources is still an important drawback.

In order to make GCPVS more competitive, many research has been done on the optimal relationship between the power capacities of all the different elements that compose them [1]. The optimal sizing of GCPVS implies an optimal relationship between the nominal or peak power of the PV generator and the nominal or maximum power of the inverter used for grid connection (see Fig. 1). The first references on this issue are dated in the 90's [2, 3] and many authors have addressed their work since then on this topic.

Fig. 1. Elements of the PV power conversion chain in a GCPVS

The most common expression employed to refer to this ratio of powers is PV-to-Inverter sizing ratio $R_S$ [7, 8, 9, 17, 19, 31 and 32]. This concept is formulated in Eq.(1), where $P_{PVG(STC)}$ (Wp) is the peak power of the PV generator measured at Standard Test Conditions (STC) (1,000 W/m2 and 25 ºC), and $P_{AC\,n}$ (W) is the nominal power of the inverter measured at the AC side under nominal conditions.

$$R_S = \frac{P_{PVG\ (STC)}}{P_{AC\ n}} \qquad (1)$$

However, there are some studies where the nominal power of the inverter is measured at the DC side [6] or were this ratio of powers is reversely defined [22, 23, 24 and 35].

Additionally, it can be found in the literature a wide variety of terms that denote the same concept, such as Inverter-to-PV array size ratio (SF) [28 and 29], Inverter-to-PV array de-rating factor (k) [44 and 45], Inverter-to-PV power ratio (r) [36], Inverter Power Ratio (IPR) [39] or Power Ratio (PR) [21 and 41], Inverter Sizing Factor (ISF) [43] and Inverter Sizing Ratio (ISR) [12, 13 and 34].

The state of the art of the optimum sizing of GCPVS is synthesized in Table 1. The structure of the table tries to summarize the key aspects of the developed research. On the one hand, the columns of the table identify the two key aspects addressed in the sizing of the GCPVS, namely, the energy yield and the economic results. In turn, these two aspects are subdivided into their main characteristic issues.

On the other hand, the Table 1 has been horizontally divided into three sections that show the main approaches to GCPVS sizing identified in the literature, namely, those only relying on simulation, those combining an experimental setup with simulation, and finally, those based exclusively on the data obtained from an experimental setup.

Each of the horizontal sections has been subdivided into five main rows that capture the essential items taken into account in the reviewed research. The first one is called “Physical characteristics of GCPVS” and refers to aspects of the facility such as the location, mounting type, orientation and tilt, irradiance, temperature, etc. The row called “Technological characteristics of GCPVS” includes aspects such as the different module technologies, inverter efficiency, sun tracking systems, shadows and data sampling. The rows "Model formulation" and "Employed software" refer to the use of a mathematical model for describing the behaviour of the GCPVS and to the specific utilized software, respectively. The row "Experimental setup" applies to those cases where a physically implemented workbench was employed.

TABLE 1

In spite of the large range of studies addressed to determine the optimal value of $R_S$, it can be considered that the basic difference between these works stems from the use or not of an experimental set up in order to clear up the problem. As mentioned above, other differential distinctive features are related to the side of the inverter where the nominal power is measured, to the employment of a reversed definition of $R_S$, to the specific model for the GCPVS used, etc.

As seen in Table 1, the studies relying only on simulation are far more abundant than those only employing data from an experimental setup or a combination of both. Also, the row "Physical characteristics of GCPVS" contains the greater number of references. This reveals that, regardless of the employed sizing approach, determining how the different location, mounting types, tilt and orientation, irradiance and temperature can affect the performance of the GCPVS has been the main issue addressed in the research.

On the contrary, the use of an experimental setup has been not so extensive. A possible explanation to the poor figures of studies employing an experimental setup or jointly integrating it with simulation lies in the difficulty to reproduce exactly in the setup the vast number of technical configurations and the different environmental conditions that can be easily applied in the simulations. All the setups reported in the examined references are specific implementations of GCPVS, which in some cases allow the possibility of varying the number of connected PV modules or changing the inverter. As a result, data obtained from these experimental setups is usually restricted to a limited number of cases and on-site conditions, which are practically impossible to replicate when desired in more than one experimental test.

Following this gap, this paper proposes a simulation technique for the determination of the GCPVS optimal value of $R_S$ in combination with an experimental setup capable of validating the model results for a wide range of technical configurations and environmental conditions. Thus, section 2 describes the problem under study, the main objectives to attain and the basic traits of the methodology applied to this aim. Next, a mathematical model for the sizing problem is formulated and the experimental setup utilized to validate the proposed approach is presented (Section 3). The environmental data and the applied processing are also described (Section 4). Then, the methodology by which the simulation and emulation processes are conducted is thoroughly explained (Section 5). Following, data from simulations and from the experimental setup are confronted and discussed (Section 6). Finally, all the factors deemed relevant for the study are duly systematized and conclusions are raised (Section 7).

## 2. Problem formulation, objectives and methodology

One of the problems traditionally encountered in the optimal sizing of the GCPVS has been the difficulty to experimentally validate the results obtained by the simulation of a great number of multiple configurations. The technical limits of the physically implemented GCPVS usually allow to replicate a small number of the simulated cases. This difficulty further increases because the environmental conditions applied in the simulation process are hardly impossible to replicate in the experimental setup.

In this regard, here it is proposed the use of a custom flexible experimental setup intended to overcome the aforementioned difficulties. It is employed in combination with a simplified model for the GCPVS based in the current state of the art. In this way, the optimal value of $R_S$ obtained from the model can be validated experimentally by means of the experimental setup.

An overview of the applied methodology is illustrated in the Figure 2. In a preliminary stage, once the setup was built and its model was formulated, several tests were carried out in the setup in order to determine the parameters needed by the model. Next, the environmental data was obtained and duly processed. Once the experimental setup and its model were fully operational, its performance was demonstrated by emulating and simulating a particular case study. Finally, the analysis and comparison of the experimental and the simulation results allowed to validate the employed model and to raise conclusions about the sizing process of the GCPVS.

Fig. 2. Overview of the applied methodology

# 3. The experimental setup and its model

## *3.1. An overview*

The proposed workbench consists of a solar array simulator (SAS), a grid-connected PV inverter and a digital power meter. A personal computer is also used as a control element for workbench management purposes. Figure 3 shows a block diagram of the proposed workbench.

Fig. 3. Block-diagram of the proposed workbench

## *3.2. Solar array simulator and PV generator model*

In the proposed workbench, the PV generator is emulated using the Agilent E4360 Modular Array Simulator operating with the E4360A power module.

The SAS operates as a PV generator with a user programmable current-voltage characteristic. This characteristic is defined by four parameters: the short-circuit current $I_{SC}$ (A), the open-circuit voltage $V_{OC}$ (V), and the current $I_{MPP}$ (A) and voltage $V_{MPP}$ (V) at the maximum power point. The E4360A power module presents some technical constraints that limit the electrical characteristics of the PV generators that can be emulated. These constraints are summarized in Table 2.

Table 2. Electrical constraints of the E4360A SAS.

The SAS used in the setup is a low power equipment (600 W) compared with the medium or large PV generators usually installed. This limitation does not lead to an important loss of generality because the rated power of the used equipment is considered in the mathematical models proposed for the description of the PV system under consideration. On the other side, the main objective of the experimental setup is the implementation of a proof of concept demonstration prototype.  However, it is always possible the series and/or parallel interconnection of low power SASs in order to emulate large PV generators.

The values of $V_{OC}$ and $I_{SC}$ needed for the SAS user programmable current-voltage characteristic are obtained by means of the PV generator model. The employed expressions are taken from the model reported in [53 and 54] and are shown in Eqs. (2), (3) and (4):

$$I_{SC} = I_{SC(STC)} \cdot \frac{H}{H_{(STC)}} \cdot \left(1 + \alpha \cdot \left(T_C - T_{C(STC)}\right)\right) \quad (2)$$

$$V_{OC} = V_{OC(STC)} \cdot \left(1 + \beta \cdot \left(T_C - T_{C(STC)}\right)\right) \cdot \left(1 + \delta \cdot \ln\left(\frac{H}{H_{(STC)}}\right)^2\right) \quad (3)$$

$$P_{PVG} = P_{PVG(STC)} \cdot \frac{I_{SC} \cdot V_{OC}}{I_{SC(STC)} \cdot V_{OC(STC)}} \quad (4)$$

Magnitudes affected by the subscript $_{(STC)}$ correspond to STC, while when not affected correspond to any operating point other than STC. $H$ and $H_{(STC)}$ are incident irradiances on the PV generator plane and $T_C$ and $T_{C(STC)}$ are temperatures of operation of the PV generator. The constants $\alpha$ and $\beta$ are the current and voltage correction coefficients for temperature, respectively, and $\delta$ is a correction coefficient for solar radiation.

The other two parameters needed for the SAS programmable current-voltage characteristic are $I_{MPP}$ and $V_{MPP}$. They can be obtained by solving iteratively the Eqs. (5), (6), (7) and (8), which are taken from [57] and complete the PV model.

$$R_{SER} = \frac{V_{OC} - V_{MPP}}{I_{MPP}} \quad (5)$$

$$\varepsilon = \frac{V_{MPP} \cdot \left(1 + \frac{R_{SER} \cdot I_{SC}}{V_{OC}}\right) + R_{SER} \cdot \left(I_{MPP} - I_{SC}\right)}{V_{OC}} \quad (6)$$

$$N = \frac{\ln\left(2-2^{\varepsilon}\right)}{\ln\left(\frac{I_{MPP}}{I_{SC}}\right)} \quad (7)$$

$$V = \frac{\frac{V_{OC}\cdot \ln\left(2-\left(\frac{I}{I_{SC}}\right)^{N}\right)}{\ln 2} - R_{SER}\cdot\left(I-I_{SC}\right)}{1+\frac{R_{SER}\cdot I_{SC}}{V_{OC}}} \quad (8)$$

In Eq. (8), *I* (A) and *V* (V) represent the current and the voltage of any operating point of the current-voltage characteristic of the PV generator. Assigning to *I* a set of values ranging between *0* and $I_{SC}$, and estimate of the complete current-voltage characteristic will be obtained. In turn, the shape of this characteristic will depend on the setting parameters $R_{SER}$ (Ω), $\varepsilon$ (dimensionless) and *N* (dimensionless) in Eqs. (5), (6) and (7), which are a function of $I_{SC}$ , $V_{OC}$, $I_{MPP}$ and $V_{MPP}$. Being $I_{MPP}$ and $V_{MPP}$ unknown, an initial guess for them must be provided to start the iterative process of resolution of the Eqs. (5)-(8). $I_{MPP}$ and $V_{MPP}$ should be adjusted iteratively until their product is consistent with the value of $P_{PVG}$ of the estimated current-voltage characteristic:

$$P_{PVG} \approx V_{MPP}\cdot I_{MPP} \quad (9)$$

A set of tests were carried out in order to compare the current-voltage characteristics obtained from the SAS with the characteristics predicted by the PV generator model. The input data for the tests correspond to a commercial PV panel with the following specifications: $I_{SC\,(STC)}$ = 4.8 A, $V_{OC\,(STC)}$ = 60.2 V, $P_{PVG\,(STC)}$ = 215 W, $\alpha$ = 0,000665 ºC $^{-1}$, $\beta$ = -0,0034 ºC $^{-1}$. The correction coefficient for solar radiation was $\delta$ = -0.04, which is a typical value for mono-crystalline Si PV panels [55]. The results are depicted in Figure 4, where dashed lines correspond to the SAS and solid lines to the PV generator model. The subplot on the left shows the characteristics obtained at $T_C$ = 25 ºC and for *H* ranging from 200 W/m$^2$ to 1000 W/m$^2$, while the subplot on the right displays the characteristics obtained at *H* = 1000 W/m$^2$ for $T_C$

ranging from 10ºC to 25 ºC. As can be seen in Figure 4, the characteristics obtained from the SAS and from the PV generator model exhibit an excellent agreement for all the tested conditions.

Fig. 4. Current-voltage characteristics from the SAS (dashed) and predicted by the PV generator model (solid), for $T_C$ = 25 ºC and different values of $H$ (left) and for $H$ = 1000 W/m$^2$ and different values of $T_C$ (right).

### *3.3. Tie grid-inverter and inverter model*

The model for the inverter when the input power is lower than the maximum inverter power is adapted from that outlined in [56]. The inverter power at the AC side $P_{AC}$ is expressed in terms of the inverter power at the DC side $P_{DC}$ as:

$$P_{AC} = \left( \frac{P_{ACn}}{P_{DCn} - P_{DC0}} - C_0 \cdot \left(P_{DCn} - P_{DC0}\right) \right) \cdot \left(P_{DC} - P_{DC0}\right) + C_0 \cdot \left(P_{DC} - P_{DC0}\right)^2 \quad (10)$$

where $P_{AC\,n}$ (W) and $P_{DC\,n}$ (W) are the nominal inverter powers at the AC side and at the DC side at nominal operating conditions, $P_{DC0}$ (W) is the minimum power at the DC side required to start the inversion process and $C_0$ (W$^{-1}$) is a parameter defining the parabolic curvature of the relationship between $P_{AC}$ and $P_{DC}$. In the model, $P_{DC}$ is assumed to be equal to $P_{PVG}$.

For input power ranges higher than the inverter maximum power, the proposed model assumes the limitation of the inverter output power to its nominal value:

$$P_{AC} = P_{ACn} \quad (11)$$

In this situation, the inverter's control unit limits the inverter input power to its maximum value (by shifting the operating point away from the maximum power point) until the overload condition is no longer present, thus ensuring the inverter output delivery with no interruptions.

The specific inverter employed in the experimental setup is the SMA Sunny Boy 700 (SB700). This device is designed for a nominal output power of 700 W and the maximum voltage and current at the DC side are 250 V and 10 A. For adequate voltage matching with the SAS, the SB700 has been configured for operation at a reduced input voltage range from 70 to

150 V, which limits the maximum current and power at the DC side to 7 A and 510 W, respectively, and the maximum power at the AC side to 460 W.

The SB700 is an inverter model adequate to the Spanish legislation (where low frequency galvanic isolation is mandatory for grid-connected devices), with a maximum efficiency around 93 % and with the behaviour of the output power limitation to the maximum value implemented.

In order to determine the parameters of the inverter model some tests were performed in the experimental setup. From the $P_{AC\,n}$ operating point specified by the manufacturer, the $P_{DC}$ received from the SAS was progressively reduced and the pair $P_{AC}$ and $P_{DC}$ was recorded. A 2nd order polynomial was fit to the obtained data, which rendered the results for the model parameters shown in Table 3. In Figure 5 it is represented the inverter efficiency, i.e. the ratio of $P_{AC}$ to $P_{DC}$, calculated from both experimental data (grey points) and the inverter model (solid black line). It is apparent the close agreement between the model and the experimental data.

Table 3. Parameters of the inverter model resulting from the 2nd order polynomial fit of experimental data

Fig. 5. Efficiency calculated from experimental data (red points) and from the inverter model (solid black line)

### 3.4. Power meter and recorder

A Yokogawa WT1600 digital power meter was used as power meter and recorder. This device monitored the voltage and current at the DC and AC sides of the inverter and recorded samples every two seconds. Data was transferred to the personal computer for further processing and permanent storage purposes at the end of each of the performed tests.

# 4. Environmental data. Solar irradiance and temperature

$P_{PVG}$ depends, among others, on the value of $H$ and the ambient temperature at the GCPVS location ($T_A$). For this study it has been considered a GCPVS located in Barcelona, Spain (41°23′N, 2°11′E), facing south and tilted 36°.

As a starting point to calculate $H$, daily horizontal radiation data for the selected location was obtained from [49]. Applying the models and correlations presented in [50], such as Erbs, Collares Pereira, Liu and Jordan and Perez, the hourly radiation at tilted surface for a representative day of each month was calculated. The day of a month whose daily radiation was the most similar to the monthly average daily radiation was selected as the representative day. This data was interpolated in periods of 15 minutes using a MATLAB® cubic interpolation function and then the resulting radiation values were expressed in terms of $H$ (W/m$^2$).

Hourly $T_A$ values were also taken from [49]. This data was monthly averaged in order to obtain the hourly $T_A$ evolution for the representative day of each month. As in the case of $H$, these results were also interpolated in periods of 15 minutes.

The $T_C$ can be modelled as in [51 and 52], namely:

$$T_C = T_A + k \cdot H \tag{12}$$

Were $k$ (°C.m$^2$/W) is a PV generator thermal coefficient called the coefficient of Ross.

The coefficient of Ross is related with the ventilation capability (natural ventilation by convection or forced ventilation by wind or airflows) and thereby depends on the PV generator mounting type. In this study it has been taken $k$ = 0.027 °Cm$^2$/W, which corresponds to the estimation carried out in [51 and 52] for not well cooled free standing PV generators mounted on flat roof.

Figures 6 and 7 show the 15-minute values of $H$ and $T_C$ for the twelve representative days of each month.

Fig. 6. 15-minute $H$ [W/m$^2$] values for the representative day of each month at selected location

Fig. 7. 15-minute $T_C$ [°C] values for the representative day of each month at selected location

# 5. Emulation and simulation processes. Proposed methodology for laboratory tests

## *5.1. Emulation process.*

Once the experimental setup had been built, characterized and validated, it was ready to be employed in the tests for the optimum $R_S$ determination of a GCPVS. The different stages of the emulation process are illustrated in the left branch of the block-diagram in Figure 8, under the label "Emulation Procedure."

FIGURE 8

Initially, the PV generator model is configured to represent a specific PV module by means of the parameters $I_{SC(STC)}$, $V_{OC(STC)}$, $P_{PVG(STC)}$, $\alpha$, $\beta$ and $\delta$. From this point, all the 15-minute interval values of $H$ and $T_C$ of the representative day of a month begin to be passed to the PV generator model. The output of the PV generator model are the parameters needed by the SAS to emulate the PV module behaviour under the specific environmental data $H$ and $T_C$, namely $I_{SC}$, $V_{OC}$, $I_{MPP}$, $V_{MPP}$. In turn, the SAS supplies the corresponding value of $P_{PVG}$ to the DC side of the inverter.

Next, the resulting $P_{AC}$ at the AC side of the inverter is sampled and recorded every 2 seconds within all the 15-minute time intervals. At the end of the test of a representative day (with an approximate duration of 7 hours, depending on the number of daily sunny hours), all the recorded data (around 12,600 samples per day) is transferred to a personal computer for further processing.

When the test is ended for the twelve representative days of a year, the annual energy delivered to the grid $E_{AC}$ is calculated according to Eq. (13):

$$E_{AC} = \sum_{1}^{m} \sum_{1}^{n_m} D_m P_{AC(n_m,m)} \cdot \Delta t \tag{13}$$

where $m$ is the ordinal of the month corresponding to a representative day ($0 \le m \le 12$), $D_m$ is the number of days of the month $m$ ($0 \le D_m \le 31$), $n_m$ is the ordinal of the $P_{AC}$ samples taken in the representative day of a month $m$, $P_{AC(nm,m)}$ is the value of the $P_{AC}$ sample $n_m$ in the representative day of the month $m$ and $\Delta t$ is the time interval between samples.

Finally, the GCPVS energy yield $Y_f$, also known as final energy yield factor, is computed in accordance with Eq. (14):

$$Y_f = \frac{E_{AC}}{P_{PVG\,(STC)}} \tag{14}$$

In order to evaluate the influence of $R_S$ on $Y_f$, a set of emulation procedures as the previously described was performed for different $R_S$ values. For the given inverter employed in the experimental setup, this involved varying $P_{PVG(STC)}$ (see Eq. (1)). The obtained results are shown at the Table 4, where a selection of the tested $R_S$ ranging from 0.85 to 1.18 is listed in its 1st column. The correspondent values of $P_{PVG(STC)}$ are shown in the 2nd column, and the $E_{AC}$ and $Y_f$ obtained in the emulation process are listed in the 3rd and 5th columns, respectively.

Table 4. $E_{AC}$ and $Y_f$ for different values of $R_{S,}$ obtained from the emulation and the simulation procedures.

### 5.2. Simulation procedure

The right branch of the block-diagram in Fig. 8 under the label "Simulation Procedure" shows the different stages of the simulation process.

The PV generator model is configured as in the emulation procedure, and the same environmental data is passed to it. Nevertheless, the output of the PV generator model needed in this case is directly the $P_{PVG}$ value to apply to the DC side of the inverter model. The inverter model renders the $P_{AC}$ at its AC side and then, $E_{AC}$ and $Y_f$ are calculated.

This simulation procedure is carried out for the same $R_S$ range considered in the emulation process, and the obtained values for $E_{AC}$ and $Y_f$ are listed in the 4$^{th}$ and 6$^{th}$ columns of Table 4.

## 6. Analysis of simulation and experimental results

Figure 9 shows the simulated results of $Y_f$ as a function of $R_S$ for a range of $R_S$ values extended to 2. The pattern of this function is basically the same regardless the values of the characteristic parameters of the considered PV system. These curves are divided into three different regions: I) Region with positive slope, where the effect of the inverter operation in low load conditions is predominant. II) Low sensitivity region, where the variation of $R_S$ has low effect over the system energy yield and where is located the optimum value of $R_S$ ($R_{S\,(OPT)}$). III) Region with negative slope, where the predominant effect is the limitation of the inverter output power.

The values of $R_S$ used in the simulation procedure cannot be reached in the emulation procedure due to the technical limits of the experimental setup. As can be seen in Table 4 and Figure 10, the emulated values of $R_S$ are ranged between 0.85 and 1.18. The effect of the inverter operation in low load conditions on the system energy yield can be seen for low values of $R_S$. Furthermore, the effect of the inverter output power limitation is not appreciable in the range of emulated values of $R_S$.

The overview presented in Figure 9 evidences a rapid decay of $Y_f$ beyond the range of $R_S$ values listed in Table 4. Accordingly $R_{S\,(OPT)}$, i.e., the optimal value of $R_S$, was estimated about 1.08.

It is noteworthy the low sensitivity of $Y_f$ to the $R_S$ values around $R_{S\,(OPT)}$. For example, the maximum value of $Y_f$ (1.6540 kWh/kW$_p$, see Table 4) experiences a reduction of less than 3% in the range of $R_S$ between 1.00 and 1.24.

Fig. 9. Simulated results of $Y_f$ as a function of $R_S$,

for a range of $R_S$ values extended to 2

On the other hand, the examination of Table 4 reveals a good agreement between the experimental and the simulation results. The 7$^{th}$ column of Table 4 presents the relative error $\varepsilon_{EAC}$ (%) among the $E_{AC}$ values obtained from the emulation and the simulation processes, which is always lower than 3 %. This relative error is also valid for the $Y_f$ values obtained from the emulation and the simulation processes, since $E_{AC}$ and $Y_f$ are directly proportional magnitudes.

The subplot on the left of Figure 10 shows the evolution of $E_{AC}$ for the limited range of $R_S$ values around $R_{S\,(OPT)}$ presented at Table 4, while the subplot on the right is devoted to $Y_f$. In both subplots, emulation results have been presented in dashed lines and simulation results in solid lines.

Fig. 10. Emulated (dashed lines) and simulated (solid lines) results of $E_{AC}$ (left subplot) and $Y_f$ (right subplots) for a range around $R_{S\,(OPT)}$

The $R_{S\,(OPT)}$ calculated from the emulation data is around 1.05, which slightly differs from the value calculated from de simulation results, namely 1.08. The relative error between both values is below 3 %.

The almost flat shape of $Y_f$ around $R_{S\,(OPT)}$ suggest that rather than seeking a precise $R_{S\,(OPT)}$ value, looking for an optimum $R_S$ interval could also be a suitable alternative approach. In the case studied in this paper the optimum $R_S$ interval could be extended near 1.2, which would imply oversizing $P_{PVG(STC)}$ respect to $P_{AC\,n}$ up to 20 %.

Additionally, it was explored the effect of the simplifying approach based on considering the most representative day of each month. To this aim, the described simulation procedure was repeated taking now into account the environmental data from the 365 days of a year rather than working with the representative day of every month. The obtained results were represented in Figure 11. While the calculated value of $R_{S\,(OPT)}$ remained the same, the convexity of the $Y_f$ curve around $R_{S\,(OPT)}$ increased. This implies that the $R_{S\,(OPT)}$ value gains relevance and the optimum $R_S$ interval is reduced. It can also be observed a reduction of the values of $E_{AC}$ and $Y_f$. Specifically, at the $R_{S\,(OPT)}$ point $E_{AC}$ and $Y_f$ approximately decreased by 6 %.

Fig. 11. Simulated values of $Y_f$ as a function of $R_S$, considering environmental data of the 365 days of a year

## *7. Conclusions*

A novel approach to the experimental validation of the $R_{S(OPT)}$ value for the $Y_f$ maximization of the GCPVS has been here presented. The implementation of a custom workbench using a SAS has allowed to overcome one of the main gaps identified in the literature at this respect, as is the scarce number of references incorporating experimental validation of the $R_{S(OPT)}$ simulation results or the limited capability of the employed setups for replicating a wide variety of technical configurations and environmental data.

The compliance between the experimental setup and the mathematical model developed to simulate the $R_{S(OPT)}$ value was demonstrated by the specific tests carried out on its two main subsystems (the PV generator and the inverter), thus the subsequent simulations were made on a firm basis. Likewise, the evaluation of the overall system also showed a good agreement between the experimental and the simulated $Y_f$ and $R_{S(OPT)}$ results, rendering relative errors below 3% for both magnitudes. The obtained results also evidenced the suitability of defining an optimum interval for $R_S$ instead of focusing on a precise value for $R_{S(OPT)}$, due to the low sensitivity of $Y_f$ to $R_S$ in the neighbourhood of $R_{S(OPT)}$. Nevertheless, this asseveration resulted somewhat tempered when more accurate environmental data was employed, since $Y_f$ results were reduced by 6%.Ultimately, the combination of the proposed simulation procedure and the custom flexible experimental setup has proved a useful tool for validating the $R_{S\ (OPT)}$ value, or alternatively the optimum $R_S$ interval, that maximizes the energetic performance of the GCPVS.

## Acknowledgements:

This work has been partially supported by the research project DPI2011-28021, Ministerio de Ciencia e Innovación (MICINN)

# References


[1] Khatib T., Mohamed A., Sopian K.. “A review of photovoltaic systems size optimizationtechniques”. Renewable and Sustainable Energy Reviews, June 2013, vol. 22, pp. 454-465

[2] Keller L., and Affolter P.. "Optimizing the panel area of a photovoltaic system, in relation to the static inverter". Proceedings of the 11th E.C. Photovoltaic Solar Energy Conference (1992), pp. 1159-1162

[3] Peippo K. and Lund P. D.. “Optimal sizing of grid-connected PV-systems for different climates and array orientations: a simulation study”. Proc. 7th International PVSEC, Nagoya, Japan (1993)

[4] Bakas P., Papastergiou K. and Norrga S.. "Solar PV array-inverter matching considering impact of environmental conditions". 37th IEEE Photovoltaic Specialists Conference (PVSC), June 2011, pp. 1779-1784

[5] Nofuentes G. and Almonacid G.. “An approach to the selection of the inverter for architecturally integrated photovoltaic grid-connected systems”. Renewable Energy, September-December 1998, vol. 15, iss. 1–4, pp. 487-490

[6] van der Borg N.J.C.M. and Burgers A.R.. "Inverter undersizing in PV systems". Proc. of 3rd World Conference on Photovoltaic Energy Conversion, May 2003, vol. 2, pp 2066-2069

[7] Notton G., Lazarov V., Stoyanov L. and Heraud N.. “Grid-connected photovoltaic system: Optimization of the inverter size using an energy approach”. 8th International Symposium on Advanced Electromechanical Motion Systems & Electric Drives (ELECTROMOTION 2009). Lille, France (2009), pp. 1-7

[8] Notton G., Lazarov V. and Stoyanov L.. “Optimal sizing of a grid-connected PV system for various PV module technologies and inclinations, inverter efficiency characteristics and locations”. Renewable Energy, February 2010, vol. 35, iss. 2, pp. 541-554

[9] Burger B. and Rüther R.. "Site-dependent system performance and optimal inverter sizing of grid-connected PV systems". Conference Record of the 31st IEEE Photovoltaic Specialists Conference, January 2005, pp. 1675-1678

[10] Burger B. and Rüther R.. “Inverter sizing of grid-connected photovoltaic systems in the light of local solar resource distribution characteristics and temperature”. Solar Energy, January 2006, vol. 80, iss. 1, pp. 32-45

[11] Song Chen, Peng Li, David Brady and Brad Lehman. “The Impact of Irradiance Time Behaviors on Inverter Sizing and Design”. IEEE 12th Workshop on Control and Modeling for Power Electronics (COMPEL 2010), June 2010, pp. 1-5

[12] Luoma J., Kleissl J. and Murray K.. “Optimal inverter sizing considering cloud enhancement”. Solar Energy, January 2012, vol. 86, iss. 1, pp. 421-429

[13] Xu Chen and Jane Melia. “Inverter size optimization for grid-connected concentrator photovoltaic (CPV) plants”. 37th IEEE Photovoltaic Specialists Conference (PVSC), June 2011, pp. 991-993

[14] Charis Demoulias. “A new simple analytical method for calculating the optimum inverter size in grid-connected PV plants”. Electric Power Systems Research, October 2010, vol. 80, iss. 10, pp. 1197-1204

[15] Kyriaki-Nefeli D. Malamaki and Charis S. Demoulias. “Minimization of Electrical Losses in Two-Axis Tracking PV Systems”. IEEE Transactions on Power Delivery, Vol. 28, No. 4, pp. 2445-.2455 October 2013

[16] http://www.trnsys.com

[17] Deb Mondol J., Yohanis Y. G. and Norton B.. “Optimal sizing of array and inverter for grid-connected photovoltaic systems”. Solar Energy, December 2006, vol. 80, iss. 12, pp. 1517-1539

[18] Deb Mondol J., Yohanis Y. G. and Norton B.. “Optimising the economic viability of grid-connected photovoltaic systems”. Applied Energy, July–August 2009, vol. 86, iss. 7–8, pp. 985-999

[19] Andreadis G., Roaf S. and Mallick T.. “Tackling fuel poverty with building-integrated solar technologies: The case of the city of Dundee in Scotland”. Energy and Buildings, April 2013, vol. 59, pp. 310-320

[20] http://www.mathworks.com/products/matlab/

[21] Islam V, Woyte A., Belmans R. and Nijs J.. “Undersizing inverters for grid connection - What is the optimum?”. Proceedings of PV in Europe, Rome, Italy (2002), pp. 780-783

[22] Velasco G., Guinjoan F., Piqué R. and Negroni J.J.. “Sizing Factor Considerations for Grid-Connected PV Systems Based on a Central Inverter Configuration”. 32nd Annual Conference on IEEE Industrial Electronics (IECON 2006), November 2006, pp. 2718-2722

[23] Velasco G., Guinjoan F., Piqué R., Conesa A. and Negroni J.J.. “Inverter power sizing considerations in grid-connected PV systems”. European Conference on Power Electronics and Applications, September 2007, pp. 1-10

[24] Velasco G., Piqué R., Guinjoan F., Casellas F. and de la Hoz J.. “Power sizing factor design of central inverter PV grid-connected systems: A simulation approach”. 14th International Power Electronics and Motion Control Conference (EPE/PEMC), September 2010, pp. 32-36

[25] Velasco G., Guinjoan F., Piqué R., Román M. and Conesa A.. Simulation-Based Criteria for the Power Sizing of Grid-Connected PV Systems. International Review on Modelling and Simulations (IREMOS). October 2011, vol. 4, n. 5, pp. 2524-2533

[26] Jiang Zhu, Brundlinge R., Betts T. R. and Gottschalg R.. "Effect of module degradation on inverter sizing". 33rd IEEE Photovoltaic Specialists Conference (PVSC '08), May 2008, pp. 1-6

[27] Sulaiman S.I., Rahman T.K.A., Musirin I.. "Novel Intelligent Sizing Algorithm for Grid-connected Photovoltaic System Design". International Review on Modelling and Simulations (IREMOS). August 2010, Vol. 3, N. 4, pp. 639-652

[28] Sulaiman S.I., Rahman T.K.A., Musirin I. and Shaari S.. "Sizing grid-connected photovoltaic system using genetic algorithm". IEEE Symposium on Industrial Electronics and Applications (ISIEA), September 2011, pp. 505-509

[29] Sulaiman S.I., Rahman T.K.A., Musirin I., Shaari S. and Sopian K.."An intelligent method for sizing optimization in grid-connected photovoltaic system". Solar Energy, July 2012, vol. 86, iss. 7, pp. 2067-2082

[30] Makhloufi S. and Abdessemed R.. "Type-2 Fuzzy Logic Optimum PV/inverter Sizing Ratio for Grid-connected PV Systems: Application to Selected Algerian Locations". Journal of Electrical Engineering & Technology (JEET), November 2011, vol. 6, n. 6, pp. 731-741

[31] Khatib T., Mohamed A., Sopian K. and Mahmoud M.. "An Iterative Method for Calculating the Optimum Size of Inverter in PV Systems for Malaysia". Przegląd Elektrotechniczny (Electrical Review), vol. 88, n. 4a/2012, pp. 281-284

[32] Khatib T.."Optimization of a grid-connected renewable energy system for a case study in Nablus, Palestine". International Journal of Low-Carbon Technologies, March 2013, pp.1–8

[33] Song Chen, Peng Li, Brady D. and Lehman B.."Optimum Inverter Sizing in Consideration of Irradiance Pattern and PV Incentives". 26th Annual IEEE Applied Power Electronics Conference and Exposition (APEC), March 2011, pp. 982-988

[34] Song Chen, Peng Li, Brady D. and Lehman B.. "Determining the optimum grid-connected photovoltaic inverter size". Solar Energy, January 2013, vol. 87, pp. 96-116

[35] Alenezi F.Q., Sykulski J.K. and Rotaru M.. "Grid-connected photovoltaic module and array sizing based on an iterative approach". SGCE International Journal of Smart Grid and Clean Energy, April 2014, vol. 3, n. 2, pp. 247-254

[36] Kil A.J. and van der Weiden T.C.J.. "Performance of modular grid connected PV systems with undersized inverters in Portugal and the Netherlands". IEEE 1st World Conference on Photovoltaic Energy Conversion, December 1994, vol. 1, pp. 1028-1031

[37] http://www.insel.eu/

[38] Keller L. and Affolter P.. "Optimizing the panel area of a photovoltaic system in relation to the static inverter-Practical results". Solar Energy, July 1995, vol. 55, iss. 1, pp. 1-7

[39] Omer S.A., Wilson R. and Riffat S.B.. “Monitoring results of two examples of building integrated PV (BIPV) systems in the UK”. Renewable Energy, July 2003, vol. 28, iss. 9, pp 1387-1399

[40] Ruther R., Knob P., Beyer H.G., Dacoregio M.M. and Montenegro A.A.. “High performance ratios of a double-junction a-Si BIPV grid-connected installation after five years of continuous operation in Brazil”. Proceedings of 3rd World Conference on Photovoltaic Energy Conversion, May 2003, vol. 3, pp. 2169-2172

[41] Gonzalez R., Jimenez H.R. and Huacuz J.M.. “Voltage and Power Ratio Effects of Grid-Connected PV Plant's Operation on the Performance Ratio and Total System Efficiency”. 3rd International Conference on Electrical and Electronics Engineering, September 2006, pp. 1-4

[42] Deb Mondol J., Yohanis Y. G. and Norton B.. “The Effect of Low Insolation Conditions and Inverter Oversizing on the Long-Term Performance of a Grid-Connected Photovoltaic System”. Progress in Photovoltaics: Research and Applications, June 2007, vol. 15, iss. 4, pp. 353-368

[43] Macedo W.N. and Zilles R.. “Operational Results of Grid-Connected Photovoltaic System with Different Inverter’s Sizing Factors (ISF)”. Progress in Photovoltaics: Research and Applications, June 2007, vol. 15, iss. 4, pp. 337-352

[44] Omar A.M. and Shaari S.. “Sizing verification of photovoltaic array and grid-connected inverter ratio for the Malaysian building integrated photovoltaic project”. International Journal of Low-Carbon Technologies, April 2009, pp. 2542-57

[45] Hussin M.Z., Omar A.M., Zain Z.M. and Shaari S.. “Sizing ratio of inverter and PV array for a-Si FS GCPV system in Malaysia's perspectives”. IEEE Control and System Graduate Research Colloquium (ICSGRC), July 2012, pp. 88-93

[46] Gregg A., Adcock C. and Brooks B.. “Optimal PV-to-Inverter Sizing Ratio”.SolarPro Magazine, April/May 2010, iss. 3.3

[47] Chourdia P.. “Optimizing Solar Panel System Efficiency through Inverter Sizing”. Solar Choice, February 2011,

[48] Fiorelli J. and Zuercher-Martinson M..“How oversizing your array-to-inverter ratio can improve solar-power system performance”.Solar Power World, July 20013, pp. 42-46

[49] SoDa Service. http://www.soda-is.com/

[50] Duffie J.A. and Beckman W.A.. “Solar Engineering of Thermal Processes”. John Wiley & Sons Inc., 3rd edition, 2006

[51] Nordmann T. and Clavadetscher L.. “Understanding temperature effects on PV system performance”. Proceedings of 3rd World Conference on Photovoltaic Energy Conversion, May 2003, vol.3, pp. 2243-2246

[52] Skoplaki E. and Palyvos J.A.. “Operating temperature of photovoltaic modules: A survey of pertinent correlations”. Renewable Energy, January 2009, vol. 34, iss. 1, pp. 23-29

[53] Smiley E., Stamenic L., Jones J.D. and Stojanovic M.. “Performance Modeling of Building Integrated PV Systems”. 16th European PV Solar Energy Conference, May 2000, pp. 39-41

[54] Skoplaki E. and Palyvos J.A..“On the temperature dependence of photovoltaic module electrical performance: A review of efficiency/power correlations”. Solar Energy, May 2009, vol. 83, iss. 5, pp. 614-624

[55] Marion B.. “Comparison of predictive models for photovoltaic module performance”. 33rd IEEE Photovoltaic Specialists Conference (PVSC '08), May 2008, pp. 1-6

[56] King D.L., Gonzalez S., Galbraith G.M. and Boyson W.E.. “Performance Model for Grid-Connected Photovoltaic Inverters”. Sandia National Laboratories Report, SAND2007-5036, September 2007

[57] Britton, Lunscher and Tanju. “A 9 kW High-Performance Solar Array Simulator”. Proceedings of the European Space Power Conference, August 1993

# Acronyms

PV: photovoltaic

GCPVS: grid connected photovoltaic systems

PV: photovoltaic

STC: Standard Test Conditions

SAS: solar array simulator

# Variables:

$C_0$: parameter defining the parabolic curvature of the relationship between $P_{AC}$ and $P_{DC}$ ($W^{-1}$)

$D_m$: number of days of the month $m$

$E_{AC}$: annual energy generated by the GCPVS (kWh)

$H$: irradiance on the PV generator plane ($W/m^2$)

$H_{(STC)}$ : irradiance on the PV generator plane at STC (1000 W/m$^2$)

$I_{MPP}$: current at the maximum power point of the PV generator (A)

$I_{SC}$: short-circuit current of the PV generator (A)

$I_{SC\,(STC)}$: short-circuit current of the PV generator at STC (A)

$k$: PV generator thermal coefficient according to the mounting type (Ross coefficient) (°C.m$^2$/W)

$m$: ordinal of the month corresponding to a representative day

$n_m$: ordinal of the $P_{AC}$ samples taken in the representative day of a month $m$

$P_{AC}$: inverter power at the AC side (W)

$P_{AC\,n}$: nominal or maximum inverter power at the AC side under nominal operating conditions (W)

$P_{AC(nm,m)}$: value of the $n_m^{th}$ $P_{AC}$ sample in the representative day of the month $m$

$P_{DC}$: inverter power at the DC side (W)

$P_{DC0}$: minimum inverter power at the DC side needed to start the inversion process (W)

$P_{DC\,n}$: nominal or maximum inverter power at the DC side under nominal operating conditions (W)

$P_{PVG}$: power of the PV generator (W)

$P_{PVG\,(STC)}$: nominal or peak power of the PV generator measured at STC (W$_p$)

$R_S$: PV-to-Inverter sizing ratio

$R_{S\,(OPT)}$: optimal value of $R_S$

$T_A$: ambient temperature of the PV generator (°C)

$T_C$: operating temperature of the PV generator (ºC)

$T_{C(STC)}$ : operating temperature of the PV generator at STC (25ºC)

$V_{MPP}$: voltage at the maximum power point of the PV generator (V)

$V_{OC}$: open-circuit voltage of the PV generator (V)

$V_{OC\,(STC)}$: open-circuit voltage of the PV generator at STC (V)

$Y_f$: energy yield or final energy yield factor (Wh/W$_p$)

$\alpha$: current correction coefficient for temperature (ºC$^{-1}$)

$\beta$: voltage correction coefficient for temperature (ºC$^{-1}$)

$\delta$: correction coefficient for solar radiation (dimensionless)

$\Delta t$: time interval between $P_{AC}$ samples [s]

Figure list:

Fig. 1. Elements of the PV power conversion chain in a GCPVS

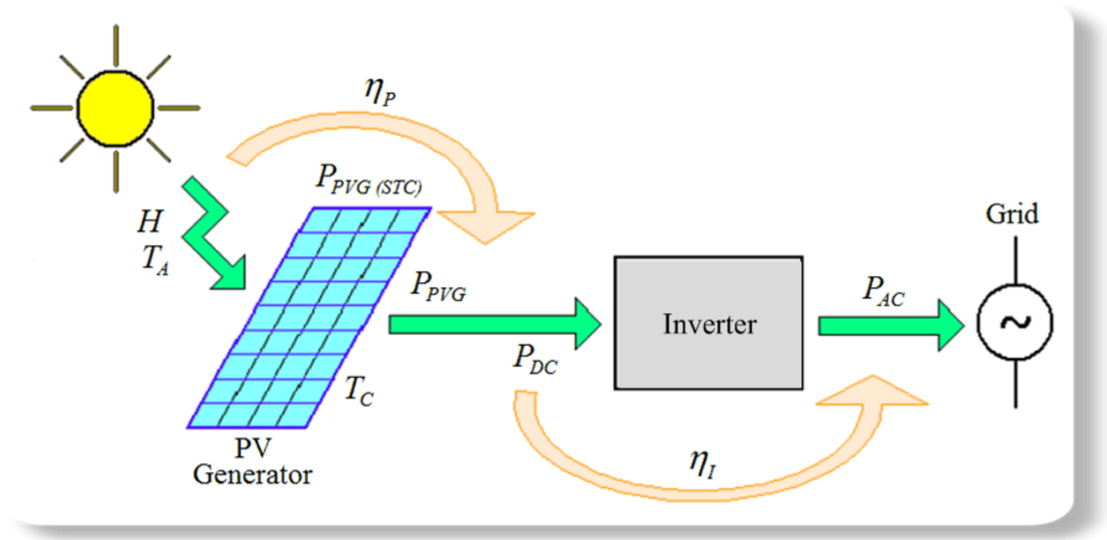


Fig. 2. Overview of the applied methodology

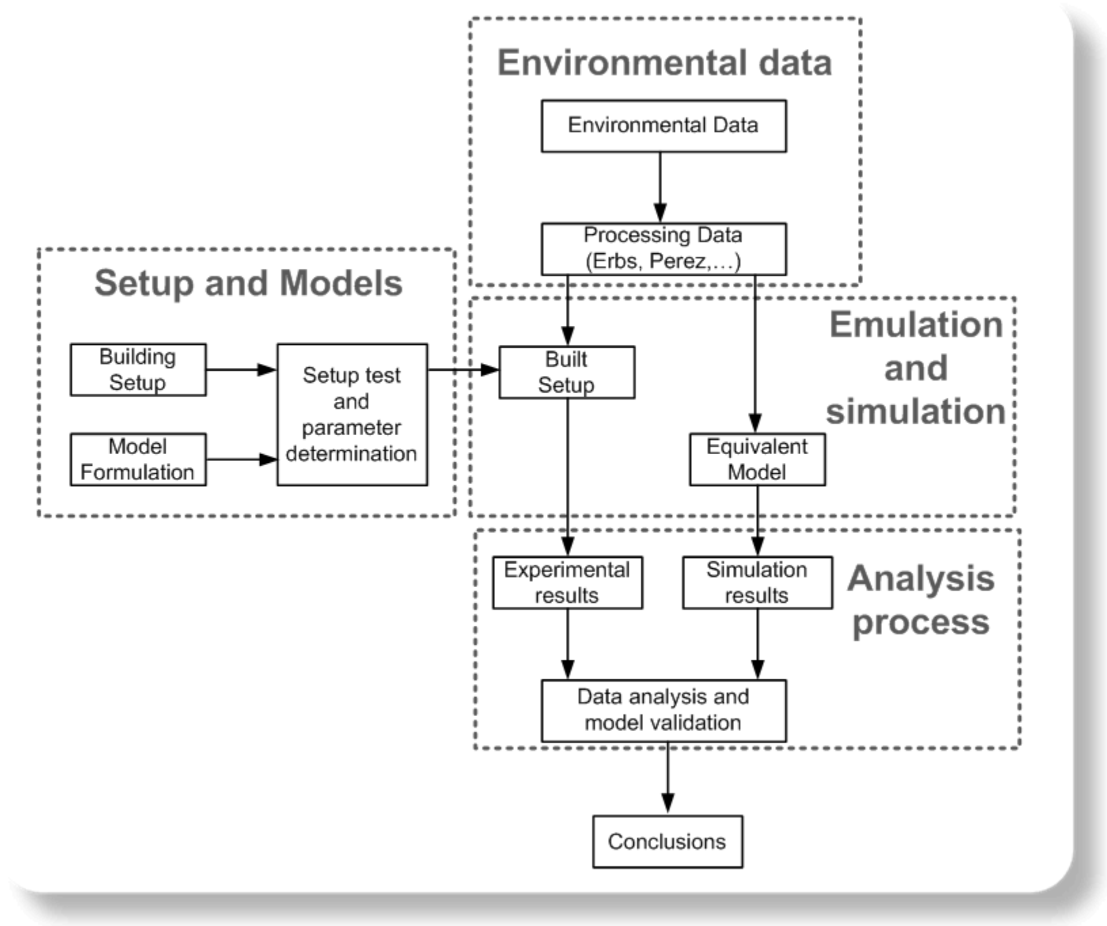


Fig. 3. Block-diagram of the proposed workbench

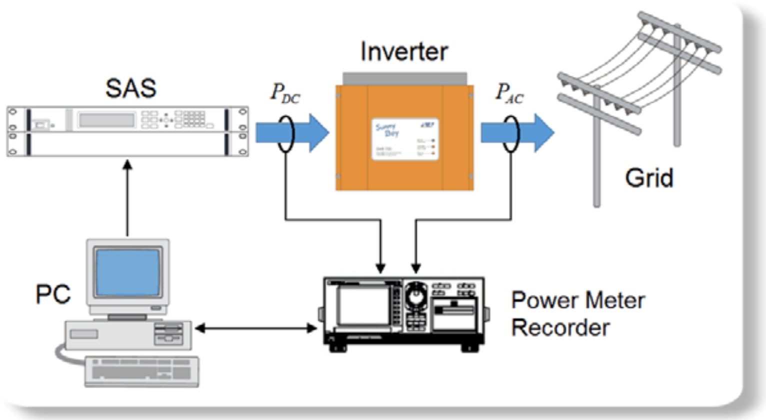


Fig. 4. Current-voltage characteristics from the SAS (dashed) and predicted by the PV generator model (solid), for $T_C$ = 25 °C and different values of $H$ (left) and for $H$ = 1000 W/m$^2$ and different values of $T_C$ (right)

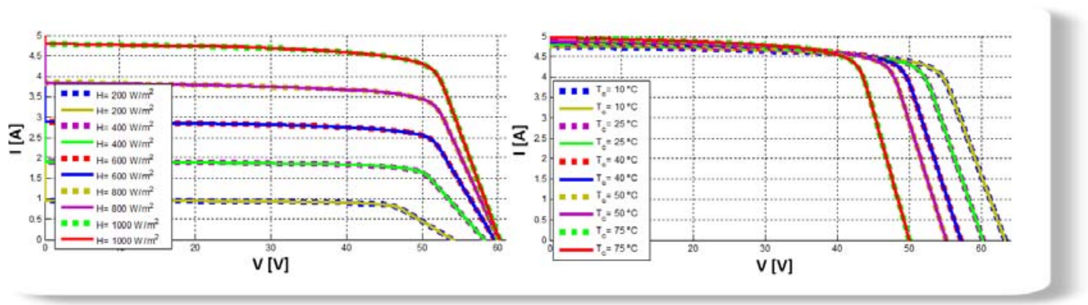


Fig. 5. Efficiency calculated from experimental data (red points) and from the inverter model (solid black line)

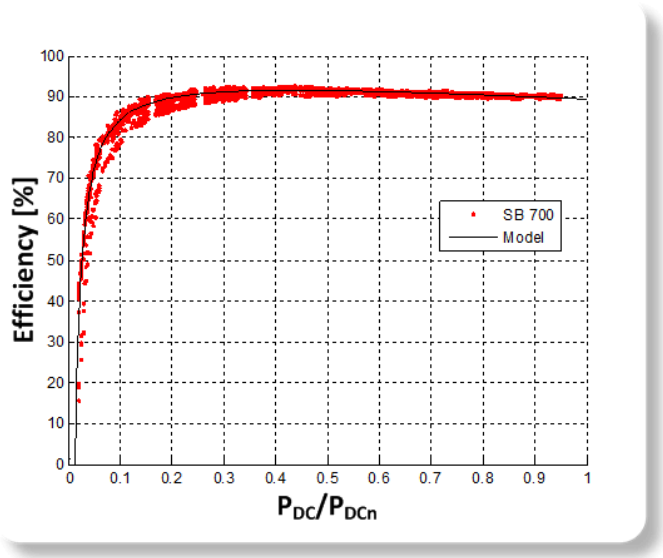


Fig. 6. 15-minute $H$ [W/m$^2$] values for the representative day of each month at selected location

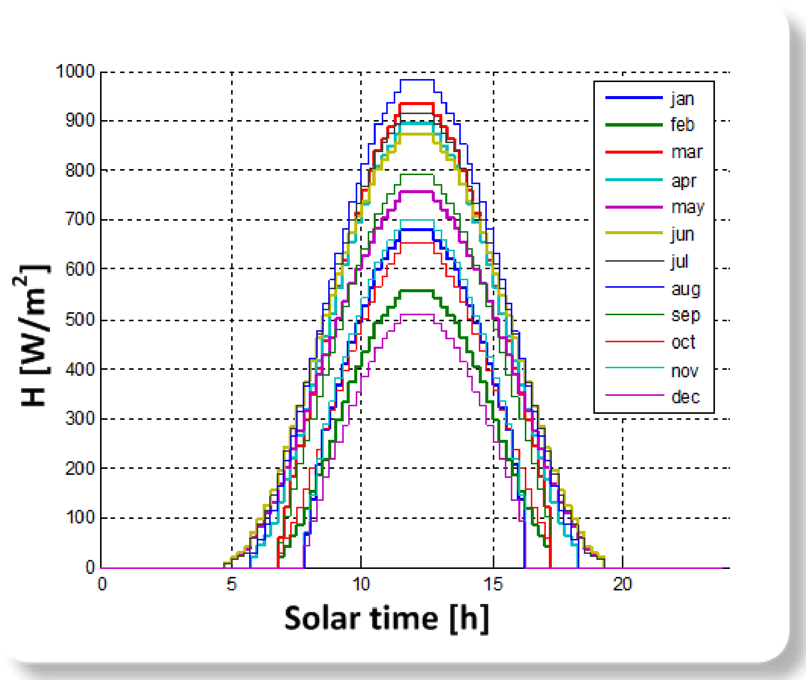


Fig. 7. 15-minute $T_C$ [°C] values for the representative day of each month at selected location

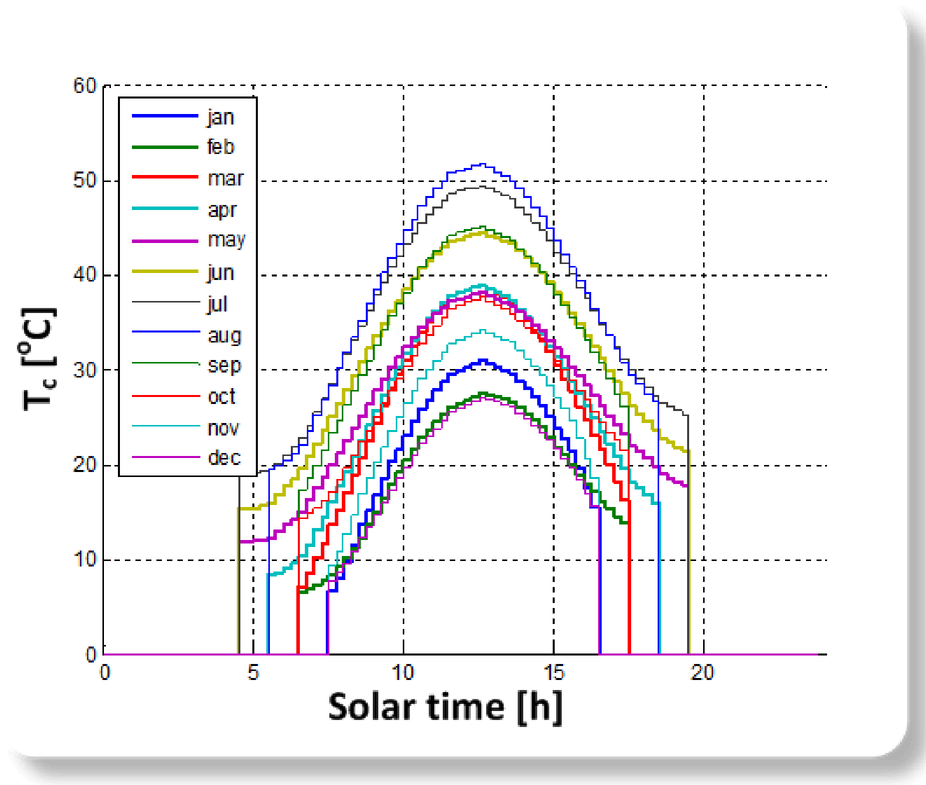


Fig. 8. Emulation and simulation procedures block-diagram

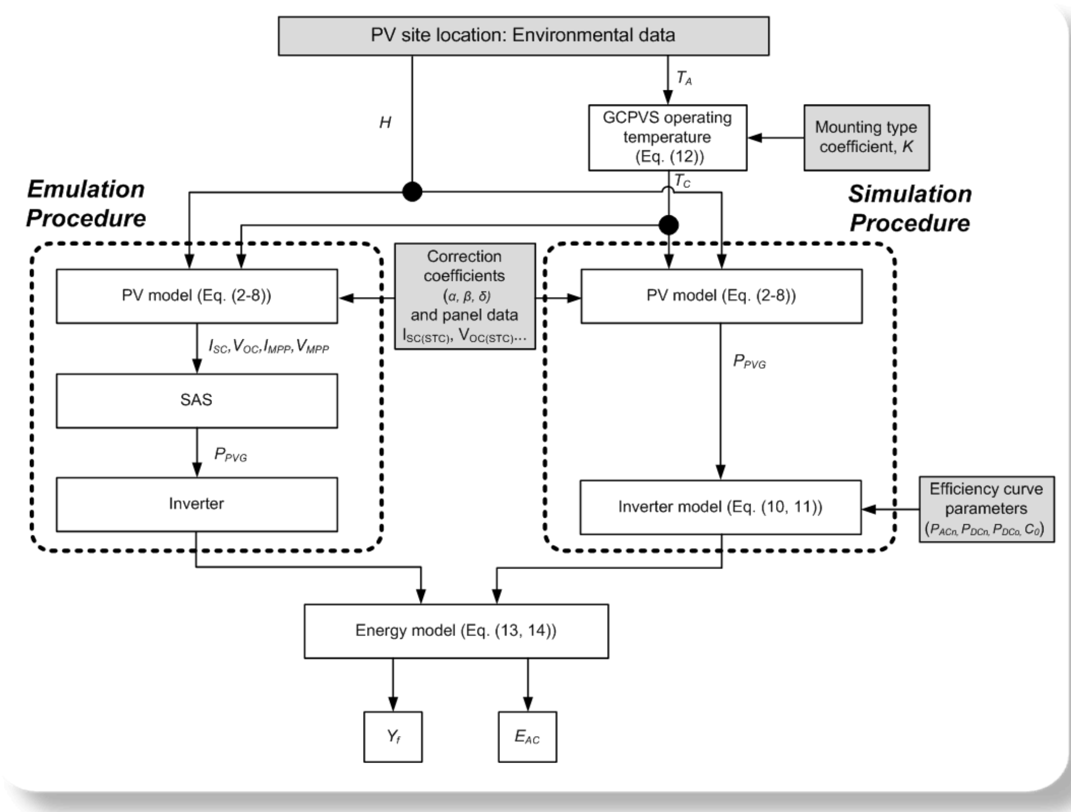


Fig. 9. Simulated results of $Y_f$ as a function of $R_S$, for a range of $R_S$ values extended to 2

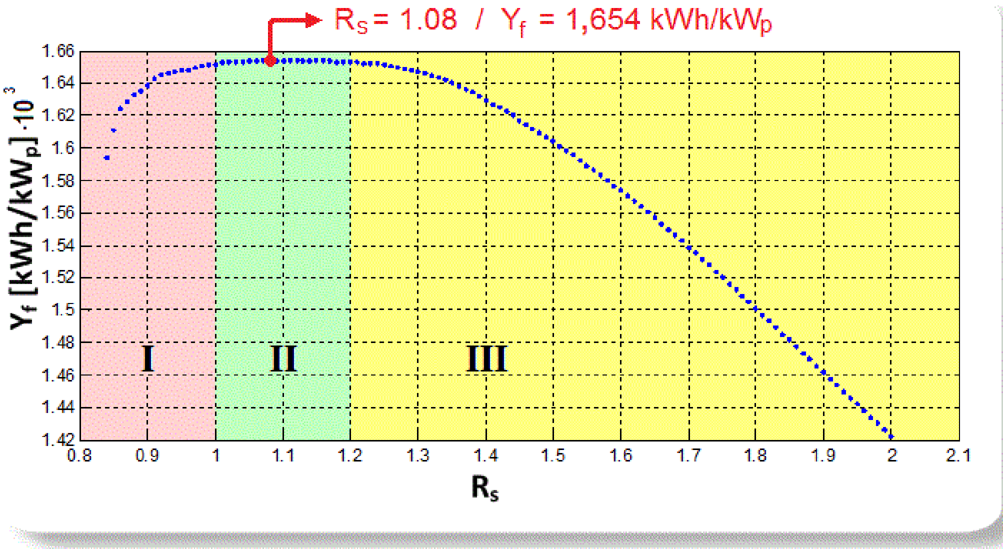

Fig. 10. Emulated (dashed lines) and simulated (solid lines) results of $E_{AC}$ (left subplot) and $Y_f$ (right subplots) for a range around $R_{S\,(OPT)}$

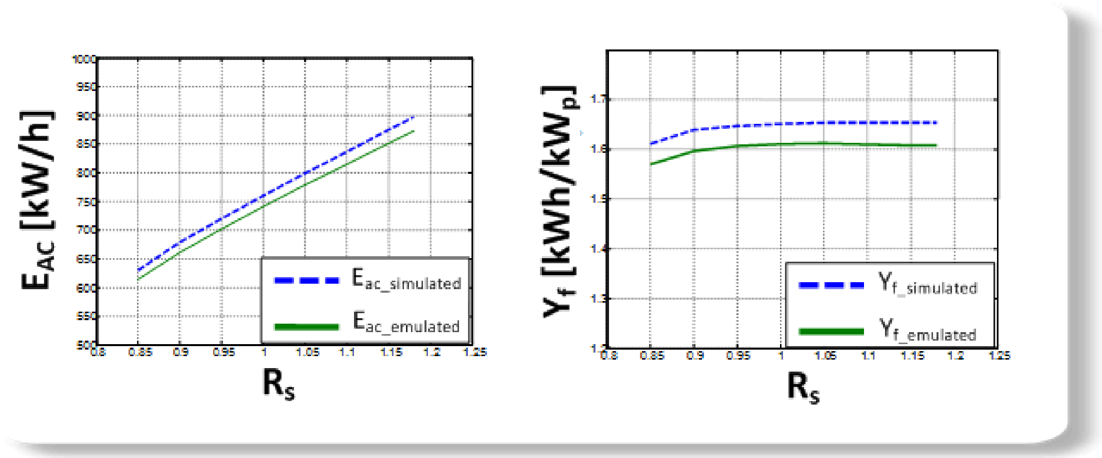


Fig. 11. Simulated values of $Y_f$ as a function of $R_S$, considering environmental data of the 365 days of a year

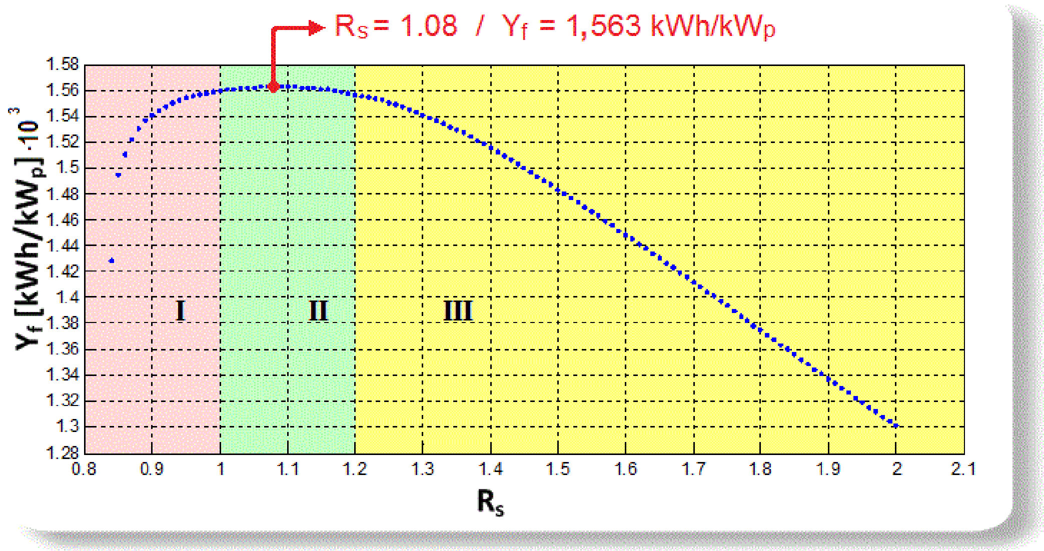

# Table list:

Table 1. Synthesized state of the art of the optimum sizing of GCPVS

| | | | Energy yield | | Economical aspects | | |
|---|---|---|---|---|---|---|---|
| | | | AC-Side | DC-Side | Life-cycle investment | Financial return | Economic performance |
| Only simulation | Physical characteristics of GCPVS | | [4, 9-15, 17-19, 21-35] | [6] | [11] | [13] | [17-19, 27, 29, 32-34] |
| | Technological characteristics of GCPVS | | [7-12, 17-19, 24-26, 33,34] | | [11] | | |
| | Model formulation | | [4, 7-15, 17-19, 21-35] | [6] | [11] | [13] | [17-19, 27, 29, 32-34] |
| | Employed software | Unspecified | [4, 7-12, 27] | [6] | [11] | [13] | |
| | | Insel | | | | | |
| | | Matlab | [15, 21-35] | | | | [27, 29, 32, 33] |
| | | TRNSYS | [17-19] | | | | [17-19] |
| | | Propietary software | [13, 14, 15] | | | | |
| | Experimental setup | | | | | | |
| | | | | | | | |
| Simulati | Physical characteristics of GCPVS | | [5, 12, 14, 36] | | | | [5] |
| | Technological characteristics of GCPVS | | [5, 36] | | | | [5] |
| | Model formulation | | [12, 14] | | | | |

| | | | | | | | | |
|---|---|---|---|---|---|---|---|---|
| on and setup | Employed software | Unspecified | [5, 12, 14] | | | | [5] |
| | | Insel | [36] | | | | |
| | | Matlab | | | | | |
| | | TRNSYS | | | | | |
| | | Propietary software | | | | | |
| | Experimental setup | | [5, 12, 36] | | | | |
| | | | | | | | |
| Only setup | Physical characteristics of GCPVS | | [38-45] | | | | [38, 39] |
| | Technological characteristics of GCPVS | | [39,44] | | | | [38, 39] |
| | Model formulation | | [43] | | | | |
| | Employed oftware | Unspecified | | | | | |
| | | Insel | | | | | |
| | | Matlab | | | | | |
| | | TRNSYS | | | | | |
| | | Propietary software | | | | | |
| | Experimental setup | | [38-45] | | | | |
| | | | | | | | |

Table 2. Electrical constrains of the E4360A SAS

| Parameter | Value |
|---|---|
| Maximum $P_{PVG}$ | 600 W |
| Maximum $V_{OC}$ | 130 V |
| Maximum $I_{SC}$ | 5 A |
| Maximum *I-V* curve slope ($\Delta V/\Delta I$) | 1 Ω |

Table 3. Parameters of the inverter model resulting from the 2nd order polynomial fit of experimental data

| **Parameter** | **Value** |
|---|---|
| $P_{AC\ n}$ | 460 W |
| $P_{DC\ n}$ | 514,66 W |
| $P_{DC0}$ | 6.37 W |
| $C_0$ | $-1.245\cdot10^{-4}$ $W^{-1}$ |

Table 4. $E_{AC}$ and $Y_f$ for different values of $R_{S,}$ obtained from the emulation and the simulation procedures

Table 4. $E_{AC}$ and $Y_f$ for different values of $R_{S,}$ obtained from the emulation and the simulation procedures.

| $R_S$ | $P_{PVG}$ (W) | $E_{AC}$ (kWh) emulated | $E_{AC}$ (kWh) simulated | $Y_f$ (kWh/kW$_P$) emulated | $Y_f$ (kWh/kW$_P$) simulated | $\varepsilon_{EAC}$ (%) $\varepsilon_{Yf}$ (%) |
|---|---|---|---|---|---|---|
| 0.85 | 391.0 | 613.79 | 629.88 | 1,569.8 | 1,610.9 | 2.62 |
| 0.90 | 414.0 | 660.79 | 678.30 | 1,596.1 | 1,638.4 | 2.65 |
| 0.95 | 437.0 | 702.06 | 719.96 | 1,606.5 | 1,647.5 | 2.55 |
| 1.00 | 460.0 | 741.20 | 759.65 | 1,611.3 | 1,651.4 | 2.49 |
| 1.05 | 483.0 | 778.56 | 798.65 | 1,611.9 | 1,653.5 | 2.58 |
| 1.08 | 496.8 | 800.28 | 821.71 | 1,610.9 | 1,654.0 | 2.68 |
| 1.15 | 529.0 | 851.12 | 874.75 | 1,608.9 | 1,653.6 | 2.78 |
| 1.18 | 542.8 | 872.75 | 897.31 | 1,607.9 | 1,653.1 | 2.81 |